

# Reactivity of Diruthenium and Dirhodium Analogues of Pentaborane(9): Agostic versus Boratrane Complexes\*\*

R. S. Anju, Dipak Kumar Roy, Bijan Mondal, K. Yuvaraj, C. Arivazhagan, Koushik Saha, Babu Varghese, and Sundargopal Ghosh\*

**Abstract:** A series of novel Cp\*-based (Cp\* =  $\eta^5$ -C<sub>5</sub>Me<sub>5</sub>) agostic, bis( $\sigma$ -borate), and boratrane complexes have been synthesized from diruthenium and dirhodium analogues of pentaborane(9). The synthesis and structural characterization of the first neutral ruthenadiborane(6) analogue are also reported. This new route offers a very efficient method for the isolation of bis( $\sigma$ -borate) and agostic complexes from diruthenapentaborane(9).

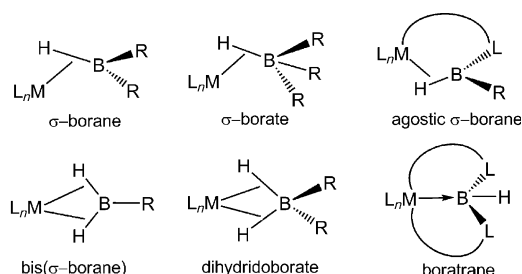
The field of transition-metal–boron chemistry, comprising a wide range of compounds from higher-nuclearity metallaborane clusters to complexes with a single boron atom, has undergone a renaissance over the past few decades.<sup>[1,2]</sup> Complexes with a wide variety of coordination modes have been isolated and structurally characterized,<sup>[1–5]</sup> for example,  $\sigma$ -borane,<sup>[3,4]</sup> boryl,<sup>[1a]</sup> and borylene complexes,<sup>[1a]</sup> metallaboranes,<sup>[1b,2]</sup> metallaboratranes,<sup>[5]</sup> and more.<sup>[1a,3c,4b]</sup> Among the various novel types recognized, the electron-precise transition-metal agostic and  $\sigma$ -borane complexes (Scheme 1), in which borane  $\sigma$ -donation to the metal center dominates over  $\pi$ -back-donation, have been a subject of regular importance.<sup>[3,4,6]</sup> However, the lack of a simple and practical

synthetic route has restricted their growth, and thus they are relatively rare, in contrast to analogous  $\sigma$ -dihydrogen and  $\sigma$ -silane complexes.<sup>[7]</sup>

Since the first example of a  $\sigma$ -borane metal complex was reported in 1996,<sup>[8]</sup> various research groups have been successful in isolating  $\sigma$ -borane/borate complexes, which turned out to be particularly useful in many catalytic hydroboration,<sup>[9]</sup> dehydrogenation,<sup>[4a,10]</sup> and C–H functionalization reactions.<sup>[10]</sup> For example, Weller and co-workers synthesized a novel bis( $\sigma$ -amine–borane) complex of rhodium by the displacement of a labile fluoroarene ligand from [Rh( $\eta^6$ -C<sub>6</sub>H<sub>5</sub>F)(P(C<sub>6</sub>H<sub>5</sub>)<sub>2</sub>( $\eta^2$ -C<sub>5</sub>H<sub>7</sub>))][BAR<sup>F</sup><sub>4</sub>].<sup>[3b]</sup> Shimoi and co-workers synthesized borane  $\sigma$ -complexes stabilized by Lewis base adducts.<sup>[6b]</sup> Subsequently, Sabo-Etienne and co-workers isolated an agostic ruthenium complex by the coordination of a potentially hemilabile boron-containing ligand to the ruthenium center.<sup>[3a]</sup> Although the metal–boron dative bond was long hypothesized, such an interaction was first authenticated by Hill et al. through the isolation of the first metallaboratrane, [M(CO)(PPh<sub>3</sub>){B(mt)<sub>3</sub>}] (M → B) (mt = methimazolyl, M = Ru and Os), in 1999.<sup>[1a,5a]</sup> In general, most established synthetic routes to these classes of compounds proceed through the coordination of a suitable boron-containing ligand to the metal center.<sup>[3–6,8]</sup> However, owing to certain limitations associated with the precursors, they are mostly restricted to the use of stable monosubstituted borane ligands, which are limited in number.

The growing number of multimetallic boron complexes containing ligands coordinated through a single boron atom<sup>[3–6,9,11,12]</sup> encouraged us to design an efficient route to  $\sigma$ - and agostic complexes that does not require the use of any preformed boron-containing ligands. In this regard, mild thermolysis of [(Cp\*<sub>2</sub>Ru)<sub>2</sub>B<sub>3</sub>H<sub>9</sub>]<sup>[13]</sup> (**1**; Cp\* =  $\eta^5$ -C<sub>5</sub>Me<sub>5</sub>) was carried out in the presence of 2-mercaptobenzothiazole (2-mbz). After the evaporation of solvent and chromatographic workup, three compounds identified as [Cp\*<sub>2</sub>RuBH<sub>2</sub>(L)<sub>2</sub>] (**2**), [Cp\*<sub>2</sub>RuBH<sub>3</sub>(L)] (**3**), and [Cp\*<sub>2</sub>RuB<sub>2</sub>H<sub>3</sub>(L)<sub>2</sub>] (**4**; L = C<sub>7</sub>H<sub>4</sub>NS<sub>2</sub>) were isolated in moderate yield (Scheme 2, see below) and fully characterized by IR and NMR spectroscopy, mass spectrometry, and X-ray diffraction studies.

The crystal structure of **2** (Figure 1 a) distinctly shows that the single boron atom is linked to the ruthenium center through a B–H–M bridge, which makes the metal–boron separation considerably longer (2.753 Å). Such an interaction can be best described as “end-on” coordination.<sup>[3a,6b]</sup> Consistent with the X-ray crystallographic results, the <sup>11</sup>B NMR spectrum of **2** contained a single boron resonance at  $\delta$  = –5.8 ppm. The <sup>1</sup>H NMR spectrum exhibited distinct signals for the metal-coordinated and terminal BH hydrogen atoms



**Scheme 1.** Various modes of metal–boron interaction.

[\*] R. S. Anju, D. K. Roy, B. Mondal, K. Yuvaraj, C. Arivazhagan, K. Saha, Dr. S. Ghosh  
Department of Chemistry, Indian Institute of Technology Madras  
Chennai, 600036 (India)  
E-mail: sghosh@iitm.ac.in

Dr. B. Varghese  
SAIF, Indian Institute of Technology Madras  
Chennai, 600036 (India)

[\*\*] This project was supported by the DST (Project No. SR/SI/IC-13/2011), New Delhi, India. IIT Madras is gratefully acknowledged for computational facilities. R.S.A. is grateful to UGC; D.K.R., K.Y., and C.A. thank the CSIR for fellowships.

Supporting information for this article is available on the WWW under <http://dx.doi.org/10.1002/ange.201310416>.

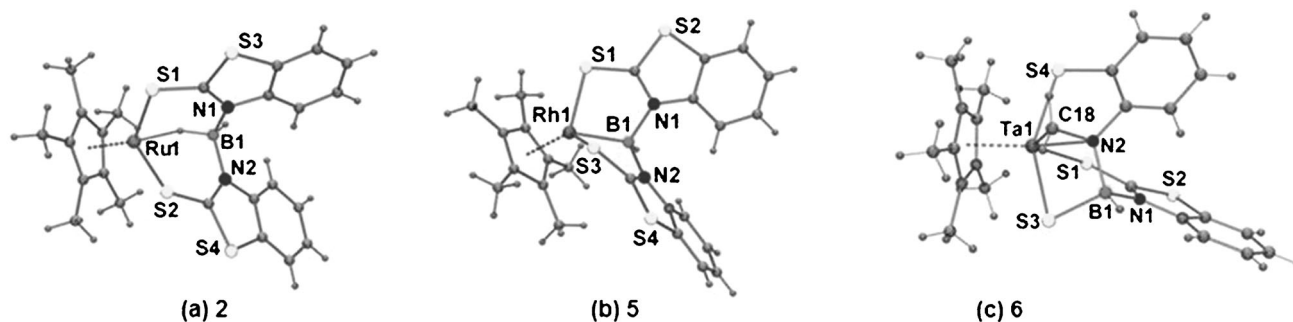


**Figure 1.** a–c) Molecular structures and labeling diagrams of **2**, **5**, and **6**. Selected bond lengths [Å]: **2**: Ru1–H2 1.830(3), B1–N1 1.563(3), Ru1–B1 2.753(1), Ru1–S1 2.336(7), B1–H2 1.160(3), S1–C1 1.675(3); **5**: Rh1–B1: 2.139(10), B1–N1 1.607(11), Rh1–S1 2.306(2), S1–C11 1.687(9); **6**: Ta1–N2: 2.176(4), B1–N2 1.559(6), Ta1–S1 2.574(12), S1–C11 1.695(6), B1–S3 1.929(6), Ta1–S3 2.393 (12), Ta1–S1 2.574 (12).

at  $\delta = -8.82$  and 6.31 ppm, respectively. The B–H bond (1.160(3) Å) coordinated to the metal center shows only marginal stretching (ca. 3.5%) relative to the terminal B–H bond (1.120(2) Å), and is thus the shortest reported B–H bond length for a three-center M–H–B unit.<sup>[14]</sup> The three-center–two-electron (3c–2e) bridge in compound **2** is tilted with a bond angle of 132°, and bisects the molecule. The two benzothiazole rings are oriented at an angle of 102° so as to minimize the steric repulsion between them. On the basis of experimental and theoretical results (see below), compound **2** can be best described as an agostic ruthenium complex with a tetracoordinate boron atom.

Structurally characterized agostic and  $\sigma$ -complexes of boron with early and late transition metals are rare.<sup>[1a,3a,4a,9]</sup> Thus, in an attempt to expand this class of complexes, we extended this approach to early (tantalum) and late (rhodium) transition metals. Thermolysis of the 2-mbz ligand with [(Cp\*Rh)<sub>2</sub>B<sub>3</sub>H<sub>7</sub>]<sup>[15]</sup> (**1**), a Rh analogue of pentaborane(9), produced compound **5** with a single boron atom. Chromatographic workup by TLC enabled us to selectively isolate and structurally characterize this novel compound as [Cp\*RhBH(L)<sub>2</sub>] (**5**). The solid-state structure of **5** (Figure 1b) shows a similar molecular structure to that of **2**, with a direct Rh–B bond (2.139(10) Å). The Rh–B bond distance in **5** is analogous to that in the first reported rhodaboratrane,<sup>[5b]</sup> [RhCl(PPh<sub>3</sub>)<sub>3</sub>{B(mt)<sub>3</sub>}] (2.132(6) Å), but longer than those observed in rhodium boryl complexes (typically in the range of 1.96–2.05 Å), and hence excludes boryl formulation. The geometry at the rhodium center can be considered as pseudooctahedral with a pentamethylcyclopentadienyl ligand. To the best of our knowledge, compound **5** is the first example of a neutral metallaboratrane in which the B(ligand)<sub>2</sub> fragment adopts a bicyclo[3.3.0] cage at a Rh center anchoring a pentamethylcyclopentadienyl ligand.

On the other hand, the reaction of 2-mbz with the tantalaborane [(Cp\*Ta)<sub>2</sub>(B<sub>2</sub>H<sub>6</sub>)<sub>2</sub>]<sup>[16a]</sup> under similar reaction conditions yielded [Cp\*TaBH(L)CH<sub>2</sub>S<sub>2</sub>NC<sub>6</sub>H<sub>4</sub>] (**6**). Structural verification by single-crystal X-ray diffraction studies showed the absence of any direct Ta–B bond or agostic interaction between Ta and the B–H bond. The molecular structure of **6** (Figure 1c) shows the presence of an azatantallacyclopropane ring (TaNC) and between the Ta and B atoms one bridging sulfide resulting from the ring opening of the heterocycle to

satisfy the 18-electron count around the Ta center. The N2–C18 bond length of 1.480(6) Å in **6** is similar to that observed in the tantallaaziridine complex [( $\eta^2$ -(N,C)-2,4,6-NC<sub>5</sub>H<sub>2</sub>Bu<sub>3</sub>)Ta(dipp)<sub>2</sub>Cl] (1.47(2) Å; dipp = 2,6-*i*Pr<sub>2</sub>C<sub>6</sub>H<sub>3</sub>).<sup>[16b]</sup> The  $\eta^2$ -coordination mode of the broken benzothiazole ligand is evident from the bond distances Ta1–C18 (2.159(5) Å) and Ta1–N2 (2.176(4) Å).

To gain some insight into the structure and bonding nature of **2**, **5**, and **6**, we carried out density functional theory (DFT) calculations.<sup>[17]</sup> The optimized structures and calculated chemical-shift values (<sup>1</sup>H and <sup>11</sup>B) closely resembled those observed experimentally (see Tables S1 and S2 in the Supporting Information). Natural-bond-orbital (NBO) second-order-perturbation-energy analysis of **2** (see Table S5) showed that the B–H  $\sigma$ -bond is slightly more polarized towards H than in the free borane–ligand adduct (see Figure S13 in the Supporting Information; 56.4 versus 51.1%). Furthermore, a strong delocalization was observed from the BH  $\sigma$ -orbital to the vacant metal orbital, rather than back-donation into the BH  $\sigma^*$ -orbital (47.9 versus 4.1 kcal mol<sup>−1</sup>; Figure 2). The result is the formation of a 3c–2e Ru...H–B bond that mostly retains the B–H character. In contrast, compound **5** shows a strong covalent Rh–B interaction with a Wiberg bond index (WBI) value of 0.67 (see

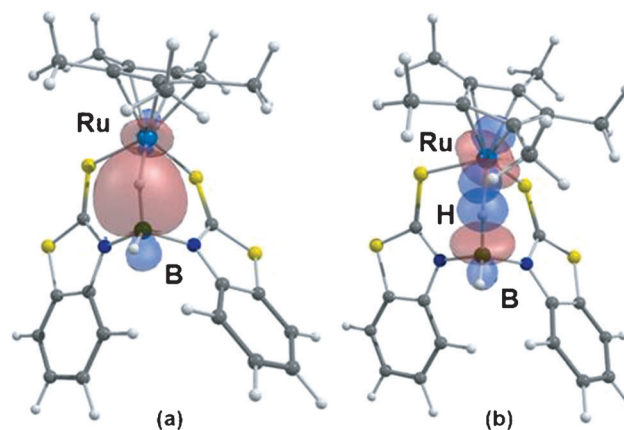


**Figure 2.** NBO donor–acceptor interaction of **2**: a)  $\sigma$ -B–H donation into a vacant orbital of Ru; b) back-bonding from Ru into the  $\sigma^*$ -orbital of the B–H bond.

Table S4 and Figure S7). Furthermore, the Ru–H–B bond in **2** has an area of charge depletion ( $-\Delta^2\rho(r) < 0$ ; see Figure S3, dashed lines) at both the Ru and the B end, whereas the H end carries a charge-concentration area ( $-\Delta^2\rho(r) > 0$ ; solid lines in Figure S3). In contrast, in **5**, an area of charge concentration was observed along the Rh–B bond only.

Compound **3**, which was isolated along with **2**, displayed a single  $^{11}\text{B}$  chemical shift at  $\delta = 8.4$  ppm. The  $^1\text{H}$  NMR chemical shifts at  $\delta = -8.40$  and 5.90 ppm were assigned to the Ru–H–B and B–H<sub>i</sub> hydrogen atoms, respectively. The solid-state X-ray crystal structure of **3** is consistent with the spectroscopic results and revealed the presence of one 2-mbz ligand. On the basis of the structure and composition of **2** and **3**, it is apparent that these molecules are technically interrelated, and that **3** could be a possible intermediate for the formation of **2**. To validate this hypothesis, we monitored the reaction of **3** with one equivalent of the 2-mbz ligand by  $^{11}\text{B}$  and  $^1\text{H}$  NMR spectroscopy. We found that under these conditions, intermediate **3** was indeed converted into agostic complex **2** with the release of hydrogen gas.<sup>[18]</sup>

The molecular structure of **3** (Figure 3a) shows the presence of a unique {Ru–S–C–N–B– $\mu\text{H}$ } metallaheterocycle. The Ru–B distance of 2.216(6) Å may be compared to that in

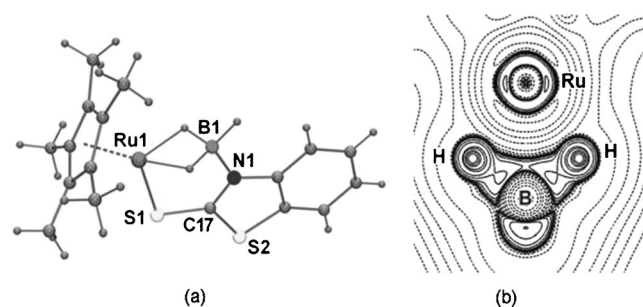


**Figure 3.** a) Molecular structure and labeling diagram of **3**. Selected bond lengths [Å]: Ru1–B1 2.216(6), B1–N1 1.514(7), Ru1–S1 2.315(16), S1–C17 1.671(5). b) Plot of the Laplacian distribution of the electron density of **3** in the Ru–BH<sub>2</sub> plane.

the hydrido(dihydroborate) complex  $[\text{RuH}\{(\mu\text{-H})_2\text{BMe-CH}_2\text{SMe}\}(\text{PCy}_3)_2]$  (2.266(8) Å; Cy = cyclohexyl).<sup>[3a]</sup> Depending on the resonance form, **3** may be considered as bis- $\sigma$  imine–borane with an anionic thiolate arm ( $\text{S}^-$ ) or a bis- $\sigma$  borate complex with a neutral thione ( $\text{C}=\text{S}$ ) arm. The bis( $\sigma$ -B–H) coordination of **3** was further supported by the Laplacian distribution  $\Delta^2\rho(r)$  in the Ru–BH<sub>2</sub> plane (Figure 3b; see also Figure S8).

Encouraged by the solid-state structures of **2** and **3**, we sought to establish the influence of the ring heteroatoms on the stability of **2** and **3** by NBO analysis. The second-order perturbation energy shows that the replacement of the ring sulfur atom with oxygen leads to less effective delocalization of the nitrogen lone pair over the thione than over the phenyl ring, thus resulting in an increased Ru–B bond distance (see Tables S5 and S6). To verify the theoretical findings, we carried out mild thermolysis of **1** with 2-mercaptobenzoxazole. As proposed, the reaction yielded  $[\text{Cp}^*\text{RuBH}_2(\text{L}')_2]$  (**2a**) and  $[\text{Cp}^*\text{RuBH}_3(\text{L}')]_2$  (**3a**;  $\text{L}' = \text{C}_7\text{H}_4\text{NOS}$ ), in which the

Ru–B bond length is considerably longer than in **2** and **3** (see Figure S1).

In parallel to the formation of the agostic complex **2** and the bis- $\sigma$ -coordinated borate **3**, the reaction of **1** and 2-mbz also yielded  $[\text{Cp}^*\text{RuB}_2\text{H}_3(\text{L})_2]$  (**4**) as a by-product. The  $^1\text{H}$ ,  $^{11}\text{B}$ , and  $^{13}\text{C}$  NMR spectroscopy and mass spectrometry data are consistent with the solid-state X-ray crystal structure (Figure 4). For example, the broad  $^1\text{H}$  chemical shifts at  $\delta =$

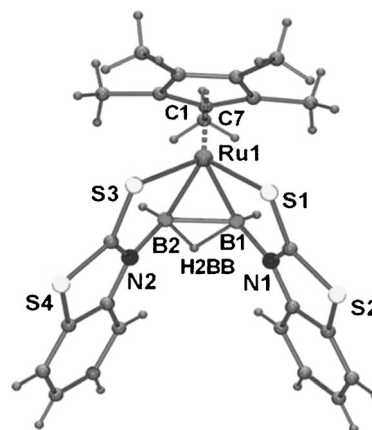


**Figure 4.** Molecular structure and labeling diagram of **4**. Selected bond lengths [Å]: Ru1–B1 2.202(3), B1–B2 1.776(4), B1–N1 1.564(3).

1.9 and 5.1 ppm suggest the presence of B–H–B and B–H<sub>i</sub> hydrogen atoms in a 1:2 ratio. As shown in Figure 4, both boron atoms are coordinated to the ruthenium atom to form an isosceles triangle with edge lengths of 1.776(4) Å (B1–B2 distance) and 2.201 Å (average Ru–B distance). A crystallographically imposed mirror plane passing through Ru1, C1, C7, and H2BB is in agreement with the presence of a single  $^{11}\text{B}$  resonance at  $\delta = 12.3$  ppm. Complex **4** may be considered as a derivative of diborane(6) in which the bridging hydrogen atom has been replaced with a  $[\text{Cp}^*\text{Ru}]$  fragment, which is thus formally bonded to the B<sub>2</sub>H<sub>5</sub> system through a single three-center B–Ru–B bond. Although meaningful discussion of the geometric parameters is limited, some of the structural features allow comparison with related species.<sup>[19,20]</sup> For example, the B–B bond length of 1.773(11) Å and the B–Ru–B bond angle of 47.53(11)° in **4** are in excellent agreement with the analogous values for the complex  $[(\eta^5\text{-C}_5\text{H}_5)\text{Fe}(\text{CO})_2(\eta^2\text{-B}_2\text{H}_5)]$ .<sup>[19]</sup> Furthermore, the molecular structure of **4** is similar to previously reported  $[(\text{CO})_2\text{-(PCy}_3)_2\text{FeB}_2\text{N}(\text{SiMe}_3)_2\text{Dur}]$ ,<sup>[20a]</sup>  $[(\text{PET}_3)_2\text{PtB}_2(\text{Dur})_2]$ <sup>[20b]</sup> (Dur = 2,3,5,6-tetramethylphenyl), and metalladiborane(4)<sup>[20c,d]</sup> complexes. Note that although the first metalladiborane(6) analogue was structurally characterized by Shore in 1989,<sup>[19a]</sup> only a handful of them are recognized.<sup>[19b]</sup>

The DFT study showed that the HOMO-1 of **4** is associated with Ru1–B1–B2 3c–2e bonding and that the LUMO + 2 is the corresponding antibonding molecular orbital (see Figure S9). The Lewis structures obtained by NBO analysis (see Figure S10) show the presence of a lone pair of electrons on each nitrogen atom that provide addi-

tional stability to **4**. Each nitrogen lone pair is significantly delocalized into the antibonding  $\pi^*$ -orbital of the phenyl ring and the thione (C=S) moiety, thus making the sulfur atom a potential donor.

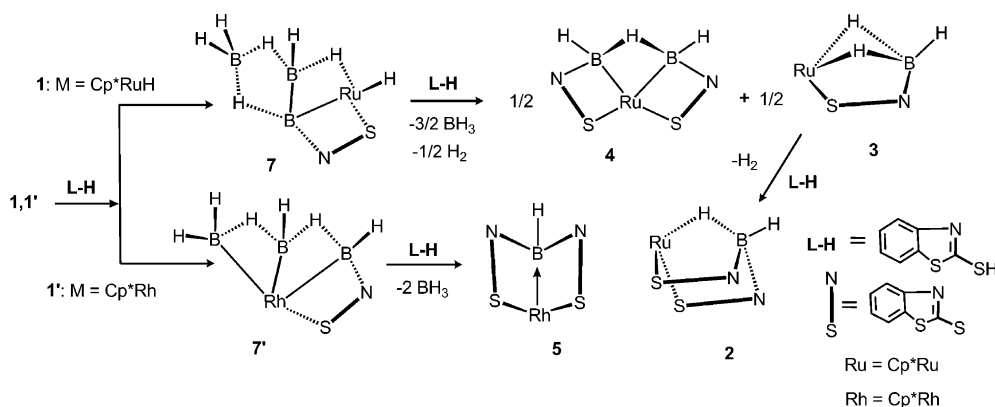
A pathway for the formation of **2–5** was unclear until the isolation of unstable intermediates  $[(\text{Cp}^*\text{M})\text{B}_3\text{H}_{6+n}\text{L}]$ , **7** and **7'** (**7**:  $n = 1$ ,  $\text{L} = \text{C}_7\text{H}_4\text{S}_2\text{N}$ ,  $\text{M} = \text{Ru}$ ; **7'**:  $n = 0$ ,  $\text{L} = \text{C}_7\text{H}_4\text{S}_2\text{N}$ ,  $\text{M} = \text{Rh}$ ), from the reaction of **1** or **1'** with 2-mbz. Intermediates **7** and **7'** might result from coordination with the 2-mbz ligand in the first step (Scheme 2). The identity of both **7** and **7'** was determined by spectroscopic studies and solid-state X-ray structure analysis of **7'**. The core structure of **7'** (Figure 5) possesses a butterfly geometry similar to that observed in tetraborane(10) and its analogues.<sup>[11,21]</sup> Furthermore, the geometry of **7'** is related to that of  $[(\text{Cp}^*\text{IrH}_2)\text{B}_3\text{H}_7]^{[21]}$  in which the replacement of the  $\text{Cp}^*\text{Ir}$  moiety by isolobal  $\text{Cp}^*\text{Rh}$

$-27.54 \text{ kJ mol}^{-1}$ ). On the other hand, the path followed by **1'** is forthright. Intermediate **7'**, generated from **1'**, yielded rhodaboratrane **5** upon further reaction with one molecule of 2-mbz, with the elimination of two molecules of  $\text{BH}_3$ .<sup>[22]</sup> All attempts to isolate an agostic Rh analogue failed.

To sum up, we have described the synthesis of an agostic ruthenium complex as well as its precursor bis- $\sigma$  borate complex and a rhodaboratrane complex by an efficient synthetic route without the use of any preformed boron-containing ligands. Our computational and synthetic results authenticate the first structurally characterized neutral ruthenadiborane(6) analogue. Investigations to evaluate the possibility of such unusual bonding situations with regard to other transition metals are under way, and we anticipate further progress in the future.

## Experimental Section

**Complexes 2–6:** In a flame-dried Schlenk tube, a mixture of compound **1** (0.13 g, 0.25 mmol) and 2-mercaptobenzothiazole (0.21 g, 1.25 mmol) in toluene (10 mL) was heated at 50 °C for 8 h. The solvent was evaporated in vacuo, and the residue was extracted into hexane and passed through Celite. Solvent was removed from the filtrate, and the residue was subjected to chromatographic workup on silica-gel TLC plates. Elution with hexane/ $\text{CH}_2\text{Cl}_2$  (90:10 v/v) yielded red **2** (0.041 g, 28%), yellow **3** (0.037 g, 35%), yellow **4** (0.015 g, 10%), and **7** (see the



**Scheme 2.** Plausible mechanistic pathway for the formation of **2–5**.

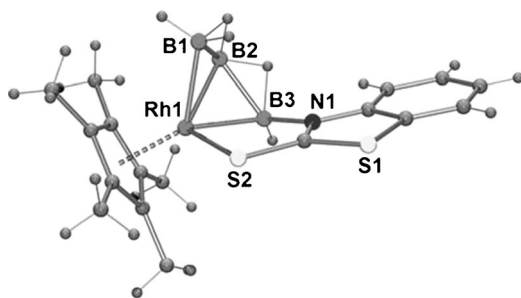


**Figure 5.** Molecular structure and labeling diagram of **7'**: Selected bond lengths [Å]: Rh1–B1 2.1765(19), B1–B2 1.801(3), B2–B3 1.820(3), Rh1–S3 2.3403(4).

fragment and the substitution of two metal hydrides ( $\text{Ir–H}$ ) and one B–H unit by the 2-mbz ligand generated **7'**.

On the basis of the composition and geometry of both **7** and **7'**, it is reasonable to assume that the second 2-mbz ligand coordinates with **7** to yield **3** and **4** with the concomitant release of  $\text{BH}_3$ .<sup>[22]</sup> Under mild thermolytic conditions, **3** further reacts with another 2-mbz ligand to afford **2** with the liberation of hydrogen gas (see above). The formation of **2** from **3** is calculated to be exergonic ( $\Delta_R G^0 =$

Supporting Information). Under similar reaction conditions, **1'** (0.13 g, 0.25 mmol) reacted with 2-mercaptobenzothiazole (0.04 g, 0.5 mmol) to yield yellow **5** (0.022 g, 15%) and **7'** (see the Supporting Information). The thermolysis of  $[(\text{Cp}^*\text{Ta})_2(\text{B}_2\text{H}_6)_2]$  (0.13 g, 0.19 mmol) with 2-mercaptobenzothiazole (0.06 g, 0.38 mmol) yielded red **6** (0.0087 g, 7%). **2**: MS (MALDI):  $m/z$  581  $[M]^+$  (isotope envelope  $\text{C}_{24}\text{H}_{25}\text{BN}_2\text{S}_3\text{Ru}$  requires 581);  $^{11}\text{B}$  NMR (128 MHz,  $\text{CDCl}_3$ , 22 °C):  $\delta = -5.8$  ppm (br, 1 B);  $^1\text{H}$  NMR (400 MHz,  $\text{CDCl}_3$ , 22 °C):  $\delta = 8.21$ – $7.23$  (m, 8 H, Ph), 6.31 (br, 1 H,  $\text{BH}_1$ ), 1.75 (s, 15 H,  $\text{Cp}^*$ ),  $-8.82$  ppm (br, 1 H,  $\text{Ru–H–B}$ );  $^{13}\text{C}$  NMR (100 MHz,  $\text{CDCl}_3$ , 22 °C):  $\delta = 149.9$  (C=N), 139.6 (CS), 130.5, 127.3, 124.9, 116.8 (Ph), 101.1 ( $\text{C}_5\text{Me}_5$ ), 10.9 ppm ( $\text{C}_5\text{Me}_5$ ); IR (hexane):  $\tilde{\nu} = 2461 \text{ cm}^{-1}$  (w,  $\text{BH}_1$ ); elemental analysis: calcd (%) for  $\text{C}_{24}\text{H}_{25}\text{BN}_2\text{S}_3\text{Ru}$ : C 49.56, H 4.34, N 4.82; found: C 50.25, H 4.07, N 4.18. **3**: MS (ESI $^+$ ):  $m/z$  416; HRMS:  $m/z$  calculated for  $^{12}\text{C}_{17}\text{H}_{22}\text{B}_1^{15}\text{N}_1^{32}\text{S}_2^{101}\text{Ru}$ : 417; found: 416.5836;  $^{11}\text{B}$  NMR (128 MHz,  $\text{CDCl}_3$ , 22 °C):  $\delta = 8.4$  ppm (br, 1 B);  $^1\text{H}$  NMR (400 MHz,  $\text{CDCl}_3$ , 22 °C):  $\delta = 8.01$ – $7.35$  (m, 4 H, Ph), 5.9 (br, 1 H,  $\text{BH}_1$ ), 1.99 (s, 15 H,  $\text{Cp}^*$ ),  $-8.40$  ppm (br, 2 H,  $\text{Ru–H–B}$ );  $^{13}\text{C}$  NMR (100 MHz,  $\text{CDCl}_3$ , 22 °C):  $\delta = 150.1$  (C=N), 139.4 (CS), 129.9, 126.1, 124.8, 116.7 (Ph), 101.2 ( $\text{C}_5\text{Me}_5$ ), 10.7 ppm ( $\text{C}_5\text{Me}_5$ ); IR (hexane):  $\tilde{\nu} = 2390 \text{ cm}^{-1}$  (w,  $\text{BH}_1$ ); elemental analysis: calcd (%) for  $\text{C}_{17}\text{H}_{22}\text{BNS}_2\text{Ru}$ : C 49.02, H 5.33, N 3.36; found: C 50.45, H 5.17, N 3.01. **4**: MS (MALDI):  $m/z$  594  $[M+\text{H}]^+$  (isotope envelope  $\text{C}_{24}\text{H}_{27}\text{B}_2\text{N}_2\text{RuS}_4$  requires 594);  $^{11}\text{B}$  NMR (128 MHz,  $\text{CDCl}_3$ , 22 °C):  $\delta = 12.3$  ppm (br, 2 B);  $^1\text{H}$  NMR (400 MHz,  $\text{CDCl}_3$ , 22 °C):  $\delta = 7.75$ – $7.40$  (m, 8 H, Ph), 5.18 (br, 2 H,  $\text{BH}_1$ ), 1.94 (br, 1 H, B–H–B), 1.60 ppm (s, 15 H,  $\text{Cp}^*$ );  $^{13}\text{C}$  NMR (100 MHz,  $\text{CDCl}_3$ , 22 °C):  $\delta = 149.7$  (C=N), 139.1 (CS), 129.4, 126.9, 124.0, 116.1 (Ph), 101.8 ( $\text{C}_5\text{Me}_5$ ), 9.7 ppm



(C<sub>5</sub>Me<sub>5</sub>); IR (hexane):  $\tilde{\nu}$  = 2437 cm<sup>-1</sup> (w, BH<sub>1</sub>); elemental analysis: calcd (%) for C<sub>24</sub>H<sub>26</sub>B<sub>2</sub>N<sub>2</sub>S<sub>4</sub>Ru: C 48.55, H 4.42, N 4.72; found: C 48.01, H 4.97, N 4.99. **5**: MS (MALDI): *m/z* 583 [M+H]<sup>+</sup> (isotope envelope C<sub>24</sub>H<sub>25</sub>BN<sub>2</sub>S<sub>4</sub>Rh requires 583); <sup>11</sup>B NMR (128 MHz, CDCl<sub>3</sub>, 22 °C):  $\delta$  = 10.2 ppm (br, 1 B); <sup>1</sup>H NMR (400 MHz, CDCl<sub>3</sub>, 22 °C):  $\delta$  = 7.82–7.15 (m, 8H, Ph), 6.32 (br, 1H, BH<sub>1</sub>), 1.66 ppm (s, 15H, Cp\*); <sup>13</sup>C NMR (100 MHz, CDCl<sub>3</sub>, 22 °C):  $\delta$  = 149.2 (C=N), 138.9 (CS), 129.1, 126.2, 123.7, 115.4 (Ph), 99.9 (C<sub>5</sub>Me<sub>5</sub>), 10.2 ppm (C<sub>5</sub>Me<sub>5</sub>); IR (hexane):  $\tilde{\nu}$  = 2416 cm<sup>-1</sup> (w, BH<sub>1</sub>); elemental analysis: calcd (%) for C<sub>24</sub>H<sub>24</sub>BN<sub>2</sub>S<sub>4</sub>Rh: C 49.49, H 4.16, N 4.81; found: C 49.07, H 4.38, N 4.57. **6**: MS (MALDI): *m/z* 662 [M+H]<sup>+</sup> (isotope envelope C<sub>24</sub>H<sub>27</sub>BN<sub>2</sub>S<sub>4</sub>Ta requires 662); <sup>11</sup>B NMR (128 MHz, CDCl<sub>3</sub>, 22 °C):  $\delta$  = 0.3 ppm (br, 1 B); <sup>1</sup>H NMR (400 MHz, CDCl<sub>3</sub>, 22 °C):  $\delta$  = 7.6–7.01 (m, 8H, Ph), 4.9 (br, 1H, BH<sub>1</sub>), 4.1 (s, 2H, CH<sub>2</sub>), 1.66 ppm (s, 15H, Cp\*); <sup>13</sup>C NMR (100 MHz, CDCl<sub>3</sub>, 22 °C):  $\delta$  = 148.7 (C=N), 133.7 (CS), 129.7, 129.2, 126.5, 122.8, 120.9, 118.3 (C=C), 61.5 (CH<sub>2</sub>), 103.3 (C<sub>5</sub>Me<sub>5</sub>), 10.6 ppm (C<sub>5</sub>Me<sub>5</sub>); IR (hexane):  $\tilde{\nu}$  = 2444 cm<sup>-1</sup> (w, BH<sub>1</sub>).

CCDC 953208 (**2**), 953206 (**3**), 953209 (**4**), 953205 (**5**), 955866 (**2a**), 955867 (**3a**), 957804 (**6**), and 953207 (**7**) contain the supplementary crystallographic data for this paper. These data can be obtained free of charge from The Cambridge Crystallographic Data Centre via [www.ccdc.cam.ac.uk/data\\_request/cif](http://www.ccdc.cam.ac.uk/data_request/cif).

Received: December 1, 2013

Revised: January 8, 2014

Published online: February 7, 2014

**Keywords:** agostic boranes ·  $\sigma$ -boranes · boratranes · rhodium · ruthenium

- [1] a) H. Braunschweig, C. Kollann, D. Rais, *Angew. Chem.* **2006**, *118*, 5380–5400; *Angew. Chem. Int. Ed.* **2006**, *45*, 5254–5274; b) T. P. Fehlner, J.-F. Halet, J.-Y. Saillard, *Molecular Clusters: A Bridge to Solid-State Chemistry*, Cambridge University Press, Cambridge, **2007**; c) H. Braunschweig, R. D. Dewhurst, V. H. Gessner, *Chem. Soc. Rev.* **2013**, *42*, 3197–3208.
- [2] D. K. Roy, S. K. Bose, R. S. Anju, B. Mondal, V. Ramkumar, S. Ghosh, *Angew. Chem.* **2013**, *125*, 3304–3308; *Angew. Chem. Int. Ed.* **2013**, *52*, 3222–3226.
- [3] a) Y. Gloaguen, G. Alcaraz, A.-F. Pécharman, E. Clot, L. Vendier, S. Sabo-Etienne, *Angew. Chem.* **2009**, *121*, 3008–3012; *Angew. Chem. Int. Ed.* **2009**, *48*, 2964–2968; b) R. Dallanegra, A. B. Chaplin, A. S. Weller, *Angew. Chem.* **2009**, *121*, 7007–7010; *Angew. Chem. Int. Ed.* **2009**, *48*, 6875–6878; c) C. Y. Tang, A. L. Thompson, S. Aldridge, *Angew. Chem.* **2010**, *122*, 933–937; *Angew. Chem. Int. Ed.* **2010**, *49*, 921–925.
- [4] a) T. M. Douglas, A. B. Chaplin, A. S. Weller, *J. Am. Chem. Soc.* **2008**, *130*, 14432–14433; b) T. D. Forster, H. M. Tuononen, M. Parvez, R. Roesler, *J. Am. Chem. Soc.* **2009**, *131*, 6689–6691.
- [5] a) A. F. Hill, G. R. Owen, A. J. P. White, D. J. Williams, *Angew. Chem.* **1999**, *111*, 2920–2923; *Angew. Chem. Int. Ed.* **1999**, *38*, 2759–2761; b) I. R. Crossley, M. R. St.-J. Foreman, A. F. Hill, A. J. P. White, D. J. Williams, *Chem. Commun.* **2005**, 221–223.
- [6] a) R. T. Baker, J. C. Calabrese, S. A. Westcott, T. B. Marder, *J. Am. Chem. Soc.* **1995**, *117*, 8777–8784; b) Y. Kawano, K. Yamaguchi, S. Miyake, T. Kakizawa, M. Shimoi, *Chem. Eur. J.* **2007**, *13*, 6920–6931; c) A. F. Hill, M. K. Smith, J. Wagler, *Organometallics* **2008**, *27*, 2137–2140.
- [7] a) G. J. Kubas, *Metal Dihydrogen and  $\delta$ -Bond Complexes*, Kluwer Academic/Plenum Publishers, New York, **2001**; b) J. Y. Corey, J. Braddock-Wilking, *Chem. Rev.* **1999**, *99*, 175–292; c) G. Alcaraz, S. Sabo-Etienne, *Coord. Chem. Rev.* **2008**, *252*, 2395–2409.
- [8] J. F. Hartwig, C. N. Muhoro, X. He, O. Eisenstein, R. Bosque, F. Maseras, *J. Am. Chem. Soc.* **1996**, *118*, 10936–10937.
- [9] “Contemporary Metal Boron Chemistry I: Borylenes, Boryls, Borane  $\sigma$ -Complexes, and Borohydrides”: T. B. Marder, Z. Lin, *Struct. Bond. (Berlin)* **2008**, *130*, 1–202.
- [10] a) J. F. Hartwig, K. S. Cook, M. Hapke, C. D. Incarvito, Y. Fan, C. E. Webster, M. B. Hall, *J. Am. Chem. Soc.* **2005**, *127*, 2538–2552; b) C. Y. Tang, N. Phillips, J. I. Bates, A. L. Thompson, M. J. Gutmann, S. Aldridge, *Chem. Commun.* **2012**, *48*, 8096–8098.
- [11] K. Geetharani, S. K. Bose, B. Varghese, S. Ghosh, *Chem. Eur. J.* **2010**, *16*, 11357–11366.
- [12] R. S. Anju, D. K. Roy, K. Geetharani, B. Mondal, B. Varghese, S. Ghosh, *Dalton Trans.* **2013**, *42*, 12828–12831.
- [13] M. G. Crestani, M. M. Hernandez, A. Arevalo, A. A. Ramirez, J. J. Garcia, *J. Am. Chem. Soc.* **2005**, *127*, 18066–18073.
- [14] S. Schlecht, J. F. Hartwig, *J. Am. Chem. Soc.* **2000**, *122*, 9435–9443.
- [15] H. Yan, A. M. Beatty, T. P. Fehlner, *Angew. Chem.* **1999**, *111*, 4630–4633; *Angew. Chem. Int. Ed.* **2001**, *40*, 4498–4501.
- [16] a) S. K. Bose, K. Geetharani, V. Ramkumar, S. K. Mobin, S. Ghosh, *Chem. Eur. J.* **2009**, *15*, 13483–13490; b) S. D. Gray, K. J. Weller, M. A. Bruck, P. M. Briggs, D. E. Wigley, *J. Am. Chem. Soc.* **1995**, *117*, 10678–10693.
- [17] Computations were performed with the Gaussian09 (rev. C.01) series of programs at the BP86 density-functional level of theory with the def2-TZVP basis set. See the Supporting Information for details.
- [18] a) G. R. Fulmer, A. J. M. Miller, N. H. Sherden, H. E. Gottlieb, A. Nudelman, B. M. Stoltz, J. E. Bercaw, K. I. Goldberg, *Organometallics* **2010**, *29*, 2176–2179; b) see the Supporting Information for experimental details.
- [19] a) T. J. Coffy, G. Medford, J. Plotkin, G. J. Long, J. C. Huffman, S. G. Shore, *Organometallics* **1989**, *8*, 2404–2409; b) J. S. Plotkin, S. G. Shore, *J. Organomet. Chem.* **1979**, *182*, C15–C19.
- [20] a) H. Braunschweig, Q. Ye, A. Vargas, K. Radacki, A. Damme, *Angew. Chem.* **2013**, *125*, 10851–10854; *Angew. Chem. Int. Ed.* **2013**, *52*, 10657–10660; b) H. Braunschweig, A. Damme, R. D. Dewhurst, A. Vargas, *Nat. Chem.* **2013**, *5*, 115–121; c) A. Wagner, E. Kaifer, H. J. Himmel, *Chem. Eur. J.* **2013**, *19*, 7395–7409; d) A. Wagner, E. Kaifer, H. J. Himmel, *Chem. Commun.* **2012**, *48*, 5277–5279.
- [21] a) L. N. Pangan, Y. Kawano, M. Shimoi, *Organometallics* **2000**, *19*, 5575–5581; b) X. Lei, M. Shang, T. P. Fehlner, *Chem. Eur. J.* **2000**, *6*, 2653–2664; c) J. Feilong, T. P. Fehlner, A. L. Rheingold, *J. Organomet. Chem.* **1988**, *348*, C22–C26; d) J. Dain, A. J. Downs, G. S. Laurensen, D. W. H. Rankin, *J. Chem. Soc. Dalton Trans.* **1981**, 472–477.
- [22] The release of BH<sub>3</sub> in the reactions was confirmed by <sup>11</sup>B and <sup>31</sup>P NMR spectroscopy of the BH<sub>3</sub>·PPh<sub>3</sub> adduct ( $\delta$  = –38.5 and 20.5 ppm, respectively). See the Supporting Information for experimental details.